

# Enclave Tasking for Discontinuous Galerkin Methods on Dynamically Adaptive Meshes \*

Dominic E. Charrier `dominic.e.charrier@durham.ac.uk`  
 Benjamin Hazelwood `benjamin.hazelwood@durham.ac.uk`  
 Tobias Weinzierl `tobias.weinzierl@durham.ac.uk`

December 9, 2021

## Abstract

High-order Discontinuous Galerkin (DG) methods promise to be an excellent discretisation paradigm for partial differential equation solvers by combining high arithmetic intensity with localised data access. They also facilitate dynamic adaptivity without the need for conformal meshes. A parallel evaluation of DG’s weak formulation within a mesh traversal is non-trivial, as dependency graphs over dynamically adaptive meshes change, as causal constraints along resolution transitions have to be preserved, and as data sends along MPI domain boundaries have to be triggered in the correct order. We propose to process mesh elements subject to constraints with high priority or, where needed, serially throughout a traversal. The remaining cells form enclaves and are spawned into a task system. This introduces concurrency, mixes memory-intensive DG integrations with compute-bound Riemann solves, and overlaps computation and communication. We discuss implications on MPI and show that MPI parallelisation improves by a factor of three through enclave tasking, while we obtain an additional factor of two from shared memory if grids are dynamically adaptive.

## 1 Introduction

Higher-order Discontinuous Galerkin (DG) techniques are part of the success story of many solvers for partial differential equations (PDEs) on supercomputers. They are considered to be guarantors for computational efficiency. Notably their fit to dynamically adaptive block-structured grids [6]—no conformity constraints are to be imposed conceptually—make them appealing. DG’s HPC selling point is that they combine high arithmetic intensity with localised, blocked data access. The combination of these two properties is a fit to predictions what exascale systems will look like [5].

For the present paper studies dynamically adaptive meshes as they result from octrees as well as generalisations and forests of those. We furthermore focus on matrix-free implicit DG methods or explicit time stepping. Their iterates or time steps, respectively, can be written down as

$$u^{(n+1)} = \left( R \circ \hat{C} + C \right) u^{(n)}. \quad (1)$$

A high order integration  $C$  of the PDE is ran strictly element-wisely. Either the outcome is subject to a Riemann solve, in this case  $\hat{C} = C$ , or the preimage is passed to the Riemann solver. The latter implies  $C = id$ . This Riemann couples adjacent cells. Both contributions are summed up and determine the next iterate  $u^{(n+1)}$ . Plain Finite Volumes skip the cell integration ( $C = \hat{C} = id$ ), while the authors from [4] use a similar formalism to study ADER-DG [7] as an example of a predictor-corrector scheme.

---

\*The authors appreciate support received from the European Unions Horizon 2020 research and innovation programme under grant agreement No 671698 (ExaHyPE).

Matrix-free or explicit methods traditionally traverse the grid to evaluate both  $C$  and  $R$ . Such traversals can be read as task graphs: The computational grid spans the graph where each task evaluates  $C$  or  $R$ , respectively, on one cell or face. Running all  $C$  tasks followed by all the Riemann solves or vice versa makes inherently bandwidth-bound steps (the  $R$  executions) take turns with the computationally demanding  $C$  evaluations. It is hence convenient to intermix the execution of  $R$  and  $C$  tasks to balance the memory pressure with the arithmetic load. Any rearrangement or parallelisation of the task execution has to be done carefully however: Dynamic adaptivity shall not be constrained despite the fact that task graphs along arbitrary resolution boundaries tend to become complicated. All prolongation and restriction along resolution boundaries has to be done in the right order. Furthermore, tasks sending and receiving MPI messages have to remain in a well-known, deterministic order. Finally, memory-intense tasks such as mesh refinement or the Riemann solves shall continuously trickle through the system to avoid memory access bursts.

We propose a novel grid traversal and task invocation paradigm which traverses the mesh. This is equivalent to running through the task graph, while we do not set up the task graph explicitly. Dynamic adaptivity would change it all the time anyway. The Riemann problems are solved during the mesh traversal whenever we load a face. They are computationally cheap and thus do not yield high throughput.  $C$  tasks in contrast are added to a background job queue. The main thread runs through the grid, executes the Riemann solves directly, but spawns the  $C$  tasks without waiting for their completion. Work stealing then deploys the computationally intense tasks from the background job queue among idle threads. We realise a producer-consumer pattern.

The approach is invalid along parallel subdomains' boundaries. Cell tasks modify the data along their faces. This face data however has to be sent out in a deterministic, consistent order. We use MPI to exchange data. For all MPI boundary cells, we do not spawn any background tasks but process them in line with the mesh traversal. Furthermore, we assume that dynamic adaptivity spreads along existing grid transitions only. It evolves smoothly in space and time. Therefore, we also exclude the cells along refinement transitions from the anarchic task execution and process them geometrically along the mesh traversal. For algorithms that have to interpolate and restrict along resolution boundaries, this makes all temporal orders well-defined and allows for a deterministic implementation of resolution-coupling operations. The result of these considerations is a totally dynamic marker-and-cell realisation over the computational mesh: All cells along MPI domain boundaries and refinement transitions are marked. Tasks on marked cells are issued directly by the mesh traversal, while all other  $C$  evaluations are deployed to (background) threads. The markers impose a skeleton mesh on top of the AMR discretisation. The skeleton's cells are processed with limited concurrency where the critical steps are done deterministically, while all other cells are subject to dynamic tasking. These other cells form enclaves. The term enclave is inspired by [20]. We could apply the enclave concept to the  $R$  tasks, too. Yet, these are not responsible for the majority of the computational cost. We thus embed them "sequentially" into the traversal which ensures that no bursts of Riemann solves can arise. Any traversal changing the grid structure can update the skeleton/enclave markers on-the-fly.

Our paper describes a geometrically inspired multitasking scheme which exploits mesh regularity and the fact that meshes typically do not change dramatically all over the domain. The idea to process "communicating cells" prior to others is, notably in the context of DG and accelerators, not new [2, 12, 20]. To the best of our knowledge, there's however no work (i) that derives and updates regularity information—the skeletons—on-the-fly, and thus imposes no constraints on the dynamic adaptivity. In our code, even the adaptivity along subdomain boundaries can change in each and every grid sweep; (ii) that transfers this "local serialisation" paradigm to dynamic adaptivity also in the shared memory context where temporal constraints are to be preserved between different resolution levels; (iii) that does not make any assumptions about the grid structure or restricts itself to particular subgrid regions/enclaves [19, 20, 12]; (iv) that works without any assembly of a task graph which becomes expensive if dynamic adaptivity makes this graph change in each and every grid



Figure 1: The logo of the ExaHyPE project underlying the present work is used as initial density passed over to the Euler equations ( $d = 2$ ). The refinement pattern follows the gradients, i.e. the spreading and diffusion of the writing, and thus makes the grid change in each and every time step. The enclaves and their skeleton thus change in every time step, too.

sweep [19, 13, 15]; and (v) that mixes tasks with different compute characteristics. We combine all of these concepts.

Enclave tasking is MPI-oblivious: As MPI data aligns along the mesh skeleton, MPI data is sent out while  $C$  jobs still might queue in the background. Therefore, sends are overlapped with computation. It is well-known that a successful realisation of data transfer behind a computation either requires regular MPI polling or a dedicated MPI communication thread. We compare a data exchange realisation which sacrifices a whole thread [9, 25, 23] for the data transfer/receive with a lazy approach where MPI probing tasks intermixed with the background jobs kick off MPI data receives as soon as incoming data becomes available. Such a lightweight approach to overlap data exchange and computation is, to the best of our knowledge, new.

There are conceptional and implementation shortcomings of the present approach. Though it does not impose any restrictions on the dynamic adaptivity, it firstly performs best in cases where the adaptivity is localised. Secondly, our data suggest that it cannot compete with standard parallel fors for regular grids. Thirdly, we propose to embed the Riemann solves into the traversal and thus to hide these bandwidth-bound operations behind the  $C$  evaluations. We sell this as one advantage of our enclave tasking. For explicit time stepping, such an approach works if and only if the time step size is known a priori or can be estimated. The authors acknowledge that often the  $C$  evaluations determine the time step size (through the CFL condition, e.g.) and it is thus difficult to merge  $C$  and  $R$  unless sophisticated time stepping with rollbacks is used. Fourthly, we note that rollbacks become mandatory if we study non-linear PDEs or non-smooth boundary conditions which “suddenly” trigger mesh refinement and thus render an identified enclave invalid. Fifthly, our case studies do not invest into load balancing or tailored task placement. Proper application of these techniques certainly will change all outcomes quantitatively.

The remainder is organised as follows: We describe our mesh and the operators of interest (Section 2) before we introduce our new enclave tasking technique in Section 3. The realisation in Section 4 describes how we tailor the tasking runtime and use MPI, before we sketch the benchmarks used (Section 5). Measurements (Section 6) uncover the potential of our approach and pick up some particular implementation lessons learned, before a conclusion summarises the main findings and sketches future work.

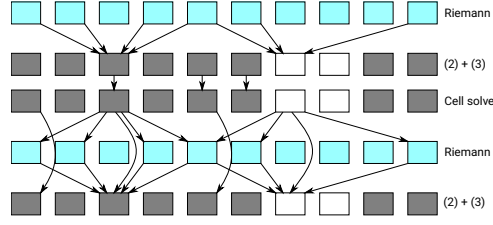


Figure 2: Schematic illustration of task graph with some dependencies for two-dimensional setup: Cells within a regular grid region (filled) combine the local DG solution with the result of  $2d$  Riemann solves. Cells adjacent to grid refinement (empty) require input from more or less Riemann solves.  $\hat{C} = C$  in (1), i.e. the  $R$  tasks pick up the result from the local solves  $C$ .

## 2 Discontinuous Galerkin on dynamically adaptive Cartesian meshes

We study DG solvers over an adaptive grid  $\Omega_h$  consisting of cells  $c$  which require us to evaluate expressions of the type

$$\int_{\Omega_h = \cup c} (\nabla \mathcal{F} u, \varphi) dx = - \sum_{\forall c \in \Omega_h} \int_c (\mathcal{F} u, \nabla \varphi) dx \quad (2)$$

$$+ \sum_{\partial c \in \Omega_h} \int_{\partial c} [[\mathcal{F} u \cdot \varphi]] dx. \quad (3)$$

The PDE with an operator  $\nabla \mathcal{F}$ , which may encode further derivatives of  $u$ , is cast into evaluations over the cells. This yields (2). As  $u$  is represented by polygons that are allowed to be discontinuous along cell faces, we obtain an additional Riemann term (3) which is integrated over all faces  $\partial c$ . Let an operator  $C$  describe (2) over the cells. The operator  $R$  summarises the Riemann solves (3).

Finite Volumes for explicit time stepping schemes choose piece-wise constant  $\varphi$  and thus cause (2) to drop out. Solely the outcome of (3) determines a subsequent time step  $u^{(n+1)} = (R + id) u^{(n)}$ . Iterative linear equation system solves based upon DG rely on residual computations where the residual comprises ingredients of the form  $(R + C) u^{(n)}$ . Their outcome determines the next iterate  $u^{(n+1)}$ . Explicit predictor-corrector schemes such as ADER-DG [7, 23] apply (2) to  $u^{(n)}$  and plug the outcome into (3). They thus yield the operator equation  $u^{(n+1)} = (R \circ C + C) u^{(n)}$ . Formalism (1) covers all three cases.

DG is popular with the supercomputing community as high order shape and test functions  $\varphi$  make the evaluation of  $C$  expensive. As both (2) and (3) rely on the same PDE terms, their arithmetic intensity [24] is comparable. We obtain a theoretical quantity of around 0.1 Flop/byte for the test bed code used in the present paper. However, the integration over  $C$  carrying polynomials which are stored as small array blocks leads to a high intensity relative to the caches [11]. At the same time, the integral (2) per cell is independent from other cells as the polygons are discontinuous.  $C$  decomposes into one task per cell. We use the symbol  $C$  for the operator and the task type synonymously, while task circumscribes an atomic work unit whose computation is independent of all other tasks. Its image only feeds into follow-up computations. Once we use reasonably high polynomial orders,  $C$  tasks become compute-bound. Operator  $R$  decomposes into one task per grid face. The individual  $R$  tasks are independent of each other. Yet, each task requires input from all adjacent cells—either an extrapolation of  $u^{(n)}$  onto the face or the projection of a  $C u^{(n)}$  outcome—and Riemann solves are modest in terms of floating point operations.  $R$  tasks are memory-bound.

The task graphs of the present DG schemes are conceptually simple (Figure 2 for (1) with  $\hat{C} = C$ ): There are cell tasks and face tasks. Cell tasks require solely the cell data as input. A cell task either is the local computation of (2) or the summation of the two contributions (2) and (3). A face task—these are the Riemann solves—requires the input data from all

adjacent cells. There are two input faces for regular grids. More cells feed into a Riemann task along adaptivity boundaries. The outcome of both task types determine the subsequent cell representation. Conceptually, it is often convenient to fuse the two types of cell tasks [4]. We thus distinguish only a generic cell task from face tasks from hereon.

The two task types translate into two grid traversal types: One over cells, one over faces. For one type of grid traversal, all  $R$  or  $C$ , respectively, evaluations are independent of each other. If the  $C$  tasks do not feed into the  $R$  tasks ( $\hat{C} = id$ ), then both types of tasks can be launched by one traversal using a producer-consumer idiom. At the end of this traversal or prior to the next traversal, we wait for all tasks to finish. The next traversal then determines the outcome of  $(R + C)u^{(n)}$ , and launches the computation of the next iterate. The traversal spawns all evaluations into a task system and deploys the decision where to launch the tasks to work stealing. No complex dependency tracking is required. We do not set up the graph, we work task assembly-free.

If  $R$  depends on  $C$ , the launch of both task types by one traversal is not trivial anymore. One option is to spawn both  $C$  and  $R$  tasks through a traversal and to make this traversal also pass all dependencies. We assemble the task graph with its dependencies on-the-fly. By the end of the grid traversal, we wait for all tasks to terminate. The subsequent traversal then brings together both ingredients, i.e. determines the outcome of  $(R \circ C + C)u^{(n)}$ , and launches the computation of the next iterate.

Task assembly-free processing becomes possible if we run over the grid twice. The first traversal issues all  $C$  tasks and eventually waits for them to complete before a second traversal issues all  $R$  tasks. Once again, summing up the ingredients of  $((R + id) \circ C)u^{(n)}$  can be integrated into the first traversal. Alternatively, we can make a traversal issue all  $R$  tasks when it reads in a face for the first time and spawn all  $C$  tasks once all  $2^d$  adjacent faces of a cell have been updated. The latter scheme relies, for explicit time stepping, on optimistic time stepping as found in [21] (see [4]). Bringing together the summands of  $((R + id) \circ C)u^{(n)}$  before we spawn the  $C$  tasks typically also determines the admissible time step size. While running a task assembly-free traversal, it might happen that some  $C$  tasks are spawned with a certain time step size which we later find out was not admissible. In this case, we need to rollback the computations performed by those tasks. The Finite Volume case ( $\hat{C} = C = id$ ) is trivial to discuss.

While we assume that our grid changes frequently, while we try to avoid the setup of any dependency graph, and while we hence focus on the first and third implementation variant, an integration of either type of DG task evaluations becomes complicated or falls short in several cases:

1. In a non-overlapping domain decomposition, cells adjacent to an MPI domain boundary contribute half of the input data for the Riemann solve. We solve the Riemann problems redundantly on both adjacent ranks. Thus the single-sided fluxes (for Rusanov, e.g.) and solutions have to be sent over to neighbouring ranks. Data exchange in MPI however has to be deterministic. We may not simply spawn  $C$  tasks or tasks that project the solution onto the faces, respectively, and then assume that the job scheduler does not permute them. There are temporal dependencies.
2. To leverage the main memory access intensity between tasks, algorithms have to avoid that all tasks access the main memory controllers concurrently, and they have to avoid cache capacity misses. A simple fire-and-forget of  $R$  and  $C$  tasks relies on the scheduler to balance between the task types. Standard schedulers from OpenMP, TBB or C++ threads will struggle to do so out of the box.
3. Many Riemann solvers on adaptive grids require the user to project the solution along resolution transitions onto the finest grid first, then to solve the formulation there, and finally to restrict the Riemann solve outcome again to the coarser grid [3]. If we run, for example, through the grid resolution levels recursively from coarse to fine grids, this is trivial to implement if we read the traversal as recursive function and plug into the backtracking. Yet, such an approach serialises mesh traversal steps: the handling of

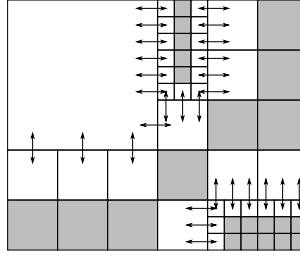


Figure 3: An adaptive Cartesian mesh where the Riemann solves along adaptivity boundaries are denoted by arrows. Cells along resolution transitions describe a grid skeleton while the filled cells form enclaves.

the coarser mesh cell has to complete before we project data down and the other way round. It imposes additional task dependencies.

4. For high sustained flop rates, it is important that no phase of the solve exhibits low concurrency, high bandwidth demands and synchronises the other tasks. Mesh cells that dynamically refine run risk to do so: If they are launched late throughout the sweep, they allocate memory, initialise data structures, and then invoke the actual computations, while the other threads might already have run out of tasks.

### 3 Enclave tasking

The approach we propose with the present paper relies on one topological assumption on the DG grid and one assumption on typical refinement patterns.

The topological assumption is common to many software packages. Let there be an initial conformal grid where each cell has roughly the same size. We assign this grid the level  $\ell_{min}$ . From this grid, we construct a finer grid by dividing each cell that we want to refine a fixed number of times equidistantly. This new grid has level  $\ell_{min} + 1$ . We continue recursively but independently for each cell. The most popular grids of this type are quadtrees and octrees as well as forests of trees [6]. Yet, also the hyperbolic ecosystem around [3] imposes such a grid topology. We use tree grids.

Our second assumption is that dynamic adaptive mesh refinement criteria refine and coarsen the mesh along resolution transitions: A cell belonging to grid level  $\ell$  might be refined if at least one adjacent cell has a level  $\hat{\ell} > \ell$ , i.e. is finer. A cell belonging to a grid level  $\ell$  might be coarsened if at least one adjacent cell has a level  $\hat{\ell} < \ell$ , i.e. is coarser. Cells surrounded by cells of the same grid level neither refine nor coarsen.

Explicit time stepping schemes for hyperbolic equation systems render our refinement/coarsening assumption reasonable as the CFL condition ensures that information such as a shock wave does not propagate more than one cell at a time. For many elliptic problems, the assumption is reasonable as users typically start with initial meshes that resolve regions of interest—typically rough regions—accurately and develop the mesh from there. Errors from “problematic” regions decay from there according to their fundamental solution, i.e. the finer grids of an appropriate mesh follow this decay. They spread from the problematic region. Refinement criteria can be throttled to refine at most one additional layer around a given region of interest which makes the dynamic refinement pattern fit to our assumption. The assumption is problematic for strongly nonlinear equations as areas of interest for a refinement criterion can be non-localised. Yet, it seems that most solvers for such problems employ sophisticated refinement criteria or domain-specific knowledge such that areas of interest are predicted and these solvers hence avoid sudden nonlocal mesh refinement.

Let a *skeleton grid* of a given adaptive mesh comprise those mesh cells that are either adjacent to a domain decomposition boundary or are adjacent to at least one cell of a different level. The remaining cells form *cell enclaves* (Figure 3).

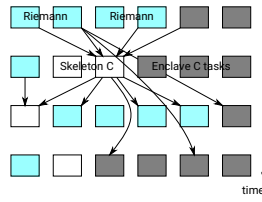


Figure 4: Schematic illustration of enclave tasking running on six cores: The code traverses a grid and processes all Riemann solves and DG solves along refinement transitions. All remaining cells’ DG problems are spawned as background tasks and processed when a core runs idle w.r.t. skeleton tasks.

Element-wise *enclave tasking* is a mesh traversal scheme which

- (a) processes all tasks associated to the skeleton grid immediately when the traversal hits them, but
- (b) spawns all tasks associated to enclaves into a task queue which is processed asynchronously by other threads.

By the end of a grid sweep, the traversal then waits for all enclave tasks to terminate, too. We parallelise the traversals themselves, which does however not compromise the present definition. An arithmetics-aware element-wise enclave tasking is a variant of this enclave tasking where only tasks of reasonable arithmetic intensity— $C$  tasks in our case—are spawned into the background. All other tasks are processed immediately agnostic of the fact whether they are member of an enclave or not. We use element-wise arithmetics-aware enclave tasking here.

The design of this tasking scheme is driven directly by the traversal characteristics and its concurrency constraints: While the enclave cell tasks  $C$  are processed non-deterministically, we run all  $R$  solves of faces when the traversal encounters a cell. There is permanently a small number of memory-intense  $R$  jobs with low arithmetic intensity trickling through the system. In return, we do not run into bursts of Riemann solves.

Cell updates and/or cell solves yield the discontinuities in the solution. For non-overlapping decompositions they have to be exchanged through MPI deterministically. As MPI boundary cells are members of the skeleton, the order of all associated  $C$  tasks is deterministic. It results from the mesh traversal order. We allow the skeleton traversal to use tasking for “its”  $C$  tasks, but the task outcomes then are merged into the mesh data and sent out deterministically.

For our assumptions, cells adjacent to those cells of differing levels might be refined or coarsened which requires memory allocations and deallocations, initialisation, and follow-up solves. Again, we allow the skeleton traversal to use tasking for the evaluation of the refinement criteria. The results however then are processed deterministically, in-order, as the handling of the resolution transitions often requires algorithm to process the varying cell resolutions in a particular order. As such cells are skeleton cells, dynamic mesh updates are interwoven into the mesh traversal, are deterministic, and never cluster at one solution point.

There are further non-functional advantageous implications of enclave tasking (Figure 4) for DG implementations. First, the skeleton’s element-wise traversal has limited concurrency. As enclave tasks are deployed to a background queue, they are supposed to slot into the schedule whenever the skeleton traversal can not exploit all hardware concurrency. Second, the pressure on the memory subsystem averages out over the traversal. Third, these skeleton cells might refine or coarsen, but as dynamic AMR is processed sequentially, we never run into bursts of memory allocations or deallocations. Notably, AMR updates never cluster towards the end of a grid traversal where no other work is left and other ranks wait for MPI data. Finally, cells triggering MPI sends belong to the skeleton and thus are, given that the enclaves are reasonably big and enclave tasks are reasonably costly, processed early throughout the traversal. This automatically allows the sends to hide behind the background tasks.

## 4 Tailoring the task runtime system

Enclave tasking proposes to rely on a producer-consumer pattern. A main thread runs through the grid and spawns all enclave work into the background while it processes all skeleton activities itself. At well-defined synchronisation points—typically the end of the current or the beginning of the next traversal—it waits for all background tasks to terminate. Such a design approach has several implications.

### 4.1 Task fusion and consumer tasks

Modern task systems such as Intel’s Threading Building Blocks (TBB) [18] are well-designed to handle millions of small tasks. In the present case, the flexibility of a graph-based task system is not required.  $C$  computations spawned are ready by construction. We instead observe that small tasks within the enclaves induce significant overhead as they poll the task system’s ready queues and suffer from NUMA [14].

To reduce the overhead, we label our enclave work items as jobs. There is a queue to which all enclave jobs are added. The TBB tasks then are job consumers pinned to one hardware thread each. They take jobs from the queue and process them. We typically launch up to  $n - 1$  of these consumer tasks if we run the code on  $n$  cores. Our code prescribes a minimum number of jobs  $J$ , i.e. a grain size, that they try to steal in one rush. This manual job stealing complements TBB’s task stealing and fuses multiple tasks/jobs. All tasks associated with skeletons are mapped onto plain TBB tasks.

### 4.2 Progressing MPI messages with early receives

Enclave partitioning ensures implicitly that partition domain boundary data is sent out early compared to work done in the interior. This holds under the assumption that the processing of the enclave  $C$  jobs requires more time than the traversal and processing of the skeleton. The approach is well-suited for non-blocking sending and thus logically overlaps sends with computation: Skeleton tasks trigger an `Isend` as soon as data becomes available while background jobs still linger in the queues. On the receiving end, we propose two more sophisticated receive strategies for enclave tasking.

Our first strategy exploits the symmetry of DG data flows. Whenever a cell sends face data to a neighbouring cell to allow this neighbouring cell’s rank to solve a Riemann problem, we know that this neighbouring cell in turn also sends in data. We solve the (cheap) Riemann problems redundantly. As a consequence, we can symmetrically issue an `Irecv` whenever we trigger a send.

Measurements suggest that, despite a timely invocation of `Irecv`, the data is not actually transferred in the background of the computation, but delayed to the next `Test` or `Wait`.

This is a well-known property of mainstream MPI implementations [9, 25]. Intel MPI therefore provides the option to dedicate one thread to the MPI data exchange. This asynchronous progress control is enabled through the flag `I_MPI_ASYNC_PROGRESS`. This resolves this issue. However, neither do many codes seem to use this feature nor are all scientists willing to sacrifice a whole thread only for MPI. Alternatively, we therefore provide a variant where consumer tasks call `Test` on all dangling receive objects whenever they run out of work.

### 4.3 A late receiver pattern

Our experimental data suggest that there are situations where it pays off to abstain from early issuing the `Irecvs`. In our second receive strategy, we do not invoke the `Irecv` explicitly within the traversal, and we accept that we run into a late sender pattern. Instead, idling threads run `Iprobes`. If an MPI probing signals that MPI messages are available, we issue an `Irecv`.

In a task language, we read the MPI probing as persistent jobs. They enqueue in the background. Once ran through, they requeue themselves. This way, we do not sacrifice a thread to MPI progression but use idle core time to implement this feature.



## 4.4 Logically blocking tasks

Our code base uses synchronous communication to coordinate the work of multiple ranks: All ranks are notified that a grid traversal has to begin, they receive time step sizes, they reduce global statistics such as the number of total grid cells, and so forth. While one could realise the underlying MPI message exchange through blocking instructions, we realise them through non-blocking operations followed by a while loop over `Test`.

This is considered to be a flaw in the MPI community. If data exchange is logically blocking, it should be realised by a blocking call instead of a non-blocking call followed by a test loop. We however consider this test loop to be equivalent to a idling consumer thread: If a logically blocking send or receive is not terminating, the thread processes some background jobs and afterwards progresses dangling MPI messages or probes the communication subsystem before it tests again.

We alter the classic multithreading role model. Many codes make a main thread bulk synchronously spawn work regions, while one thread is reserved for the MPI communication. Our main thread feeds the other threads with work. Once it finishes or runs into a logically blocking MPI routine, it helps out to finish the work plus actively polls or progresses MPI.

## 5 Benchmark application

To evaluate the potential of our enclave tasking, we make (1) model the compressible Euler equations solved through explicit time stepping. The equation

$$\partial_t u + \nabla \mathcal{F} u = 0 \quad (4)$$

with five unknowns

$$\begin{aligned} u &= (\rho, j_1, j_2, j_3, E)^T =: (\rho, j, E)^T \text{ and} \\ \mathcal{F} u &= \begin{pmatrix} j \\ \frac{1}{\rho} j \otimes j + p \cdot id \\ \frac{1}{\rho} j (E + p) \end{pmatrix} \end{aligned}$$

is closed by the pressure constraint equation  $p = 0.4 \left( E - \frac{1}{2\rho} (j, j) \right)$ .  $\rho$  is the medium density,  $E$  the energy,  $j$  is the vector field of the velocities. This standard benchmark [16] is supplemented by initial conditions (Figure 1) which are smooth enough not to yield shocks but varying enough to make dynamic AMR per time step convenient.

We discretise the computational domain with a standard spacetree data structure: It is a spacetree where each cell is subdivided into three parts per coordinate axis when we refine from level  $\ell$  into  $\ell + 1$ . Three-partitioning is advantageous for Finite Volumes-type codes: Whenever we refine, the cell centre of the old coarse cell coincides spatially with a cell centre of a refined cell. All grid construction is constrained by a minimal level  $\ell_{min}$  and a maximum level  $\ell_{max}$ , i.e. a finest mesh size. Into the leaves of our tree, we embed Lagrange polynomials spanned by Gauss-Legendre points. We cover polynomial orders  $p \in \{3, 6, 9\}$ . With five unknowns, the solution per cell is spanned by  $5(p+1)^3$  doubles for our three-dimensional setup.

The explicit time stepping is based upon an ADER-DG formalism [7, 23]. For a detailed discussion of the scheme, we refer to respective literature, and instead put emphasis on the realisation properties of the individual steps. (i) The weak cell-wise problem (2) is solved in space and time. As (4) is non-linear, we employ a Picard iteration where the iteration count is constrained to  $p + 1$ . The  $C$  tasks are computationally demanding. (ii) We use a plain Rusanov [16] solver along the faces for (3). The outcome of  $C$  feeds into these Rusanov solvers, i.e. we solve a predictor-corrector system  $(R \circ C)u^{(n)}$ . (iii) The contributions of both  $C$  and  $R$  tasks are summed up which yields the next time step. We work with global time stepping and known time step sizes. Thus, we can make the summation  $u^{(n+1)} = (R \circ C + C)u^{(n)}$  a

Table 1: The benchmark’s characteristics on one Broadwell core. Bandwidth in MBytes/s. We report the arithmetic intensity (AI) as flop/byte, show both the value relative to the L1 accesses [24] and the measured value relative to the main memory data transfer [11].

order	Mflop/s	Bandwidth	AI vs. mem	AI vs. L1
3	1464.35	568.18	2.38	0.08
6	2893.11	388.90	6.73	0.10
9	3111.02	199.60	14.28	0.11

preamble of the subsequent  $C$  solves. (iv) Our code relies on gradient-based refinement, where the mesh is coarsened if the solution is very smooth, while it refines as soon as one gradient of the five unknowns exceeds a prescribed threshold. (v) Finally, all data reported comprises both the AMR and the whole time stepping. It however neglects cost of grid setups, and it switches off further features such as IO. For distributed memory setups where we use a non-overlapping domain decomposition from a cells’ point of view: While there’s no redundancy among the cells, each Riemann solve along the domain boundaries is performed twice as the ranks exchange the Riemann solve’s input and then determine the outcome redundantly. We ensure that we measure over short simulation time spans (ten time steps) where all work is reasonably balanced.

Our choice of a testbed is rigorous. First, the code/measurements are stripped off all features that are not directly affected by enclaving (load balancing or IO, e.g.) and we study a simple PDE. Second, our testbed sticks, for a HPC case study, to low polynomial orders. Other reports easily exceed a polynomial order of  $p = 10$  [10] and thus end up in a regime strongly dominated by computations. Third, we study a very simple PDE which results in low flop counts. As a result, we obtain cheap/bandwidth-bound Riemann tasks with an arithmetic intensity of only around 0.1, while we clearly see the impact of the implicit, per-cell cache blocking of DG resulting in a way higher intensity relative to the main memory accesses (Table 1).

We end up with a setup where the task system has to cope with many tasks of completely different compute characteristics. Finally, few real-world setups will require an excessive flexibility where the grid changes in each and every time step. The overall experimental choices are unforgiving for the enclave tasking and uncover its potential. As drawback, we have to leave it to the reader to put all achievements in perspective for particular real-world applications with more complex performance determinands, different baseline characteristics (order or computational load, e.g.) and further features interfering with the time to solution.

## 6 Experimental results

Three systems are used to evaluate our methodology. We conducted our experiments on

1. an Intel E5-2650 v4 (Broadwell) cluster with  $2 \times 12$  cores per node. They run at 2.20 GHz and are connected by Omnipath. All hardware counters measurements have been done on this system through Likwid [22].
2. an Intel Xeon E5-2697 v3 (Haswell) cluster with  $2 \times 14$  cores. They run at 2.60GHz and are connected by Infiniband.
3. a KNL (Xeon Phi 7210F) cluster with 64 cores per node, configured in the quadrant clustering mode. They run at 1.30 GHz. Its High Bandwidth Memory is used as cache.

For all shared memory parallelisation, we rely on Intel’s Threading Building Blocks (TBB) while Intel MPI is used for the distributed memory parallelisation. Intel’s 2017 C++ compiler translated all codes.

The performance/comparison baseline for our tests is a serial run with neither MPI nor TBB support compiled in. To challenge our realisation, we always compare our code to a plain parallel for-based code. If this comparison code encounters adaptive meshes, it splits

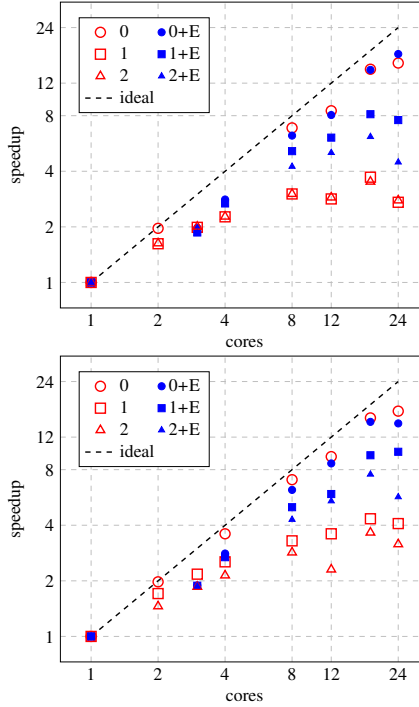


Figure 5: Shared memory speedup on Broadwell without vs. with (label +E) enclave tasking. All data are normalised against a serial run without any enclave reordering. We use polynomial order  $p = 6$  (top) and  $p = 9$  (bottom), while the numerical labels denote  $\Delta\ell = \ell_{max} - \ell_{min}$ , i.e. the AMR constraints. A zero index denotes a regular grid.

up these meshes into regular subgrids, processes the subgrids one after another, processes the resolution interfaces serially, and runs through each regular grid with a parallel for [?].

If not stated otherwise, all experiments start from with a  $27 \times 27 \times 27$  grid which yields 1,259,712 ( $p = 3$ ), 6,751,269 ( $p = 6$ ) or 19,683,000 ( $p = 9$ ) degrees of freedom (dofs). To this grid, we add additional AMR grid levels  $\Delta\ell > 0$ . For  $\Delta\ell = 1$ , this increases the dof count by a factor of 1.30, for  $\Delta\ell = 2$  we scale the original number of dof by 2.66. For  $\Delta\ell = 3$ , we finally end up with 7.07 times the regular count.

## 6.1 Background job configuration

We start our experiments with a brief study of how to configure the background job processing, and validated experimentally (not shown) that  $J = 0$  yields runtimes close to a realisation where we model all  $C$  jobs as TBB tasks.

For enclave tasking it however seems to be ill-suited to have one thread spawning all tasks and all other threads stealing from this one [17]. Native TBB gives enclave tasks too much priority. We therefore (i) enqueue all enclave jobs into a queue manually, (ii) allow only up to  $\#cores/2$  TBB tasks to consume these jobs throughout the traversal, (iii) make a consumer tasks always steal at least  $J = 4$  jobs in one rush, and (iv) finally use  $\#cores - 1$  consumer tasks once the skeleton is processed.

## 6.2 Multicore shared memory scalability

Runs of enclave tasking on a single Broadwell node (Figure 5) reveal that the administration of the  $C$  tasks in a queue and their eventual processing is not for free. It does not compromise the serial performance significantly, but it makes enclave tasking perform poorer than a plain parallel for on regular grids.

Table 2: Broadwell performance counters.  $\Delta\ell = \ell_{max} - \ell_{min}$ . Bandwidth data is given as Mbytes/s and data volume as Gbytes. The +E marker denotes the usage of enclave tasking.

$p$	$\Delta\ell$	cores	L2 miss rate	Mem. bandwidth	Mem. volume
3	0	1	0.0003	438.6	11.9
		1+E	0.0024	545.2	15.0
		12	0.0143	2001.7	13.2
		12+E	0.0032	2685.0	16.5
		24	0.0048	4270.4	30.6
		24+E	0.0023	5588.8	31.8
3	1	1	0.0036	303.5	11.1
		1+E	0.0021	432.8	15.6
		12	0.0068	275.1	11.3
		12+E	0.0062	483.1	11.3
		24	0.0096	4391.8	249.2
		24+E	0.0085	4684.0	201.6
6	0	1	0.0081	117.8	47.2
		1+E	0.0078	148.5	59.2
		24	0.0082	2915.5	74.8
		24+E	0.0167	3222.5	103.2
6	1	1	0.0077	105.7	45.5
		1+E	0.0081	140.3	60.7
		24	0.0087	1935.1	332.5
		24+E	0.0078	3018.4	247.3

The baseline code scales well for regular grids. Once dynamic adaptivity kicks in, its performance degrades. With AMR, enclave tasking outperforms the baseline code. It unfolds its full potential for dynamically adaptive grids where it succeeds in keeping the cores busy.

We continue to see a deterioration of scalability with vast, non-localised adaptivity almost tripling the dof count. Every additional level of adaptivity increases the ratio of skeleton cells to enclave cells and thus makes the ratio of background to skeleton cells worse. In turn, the impact of enclave tasking improves with an increasing polynomial order, i.e. with an increase of the computational load of the  $C$  tasks compared to the AMR cost and the Riemann solves.

While the code overall is cache efficient (Table 2)—the omitted L3 cache hit rate resembles the L2 cache hit rate—we see that enclave tasking increases both memory bandwidth and total memory amount transferred through the memory controllers. While the observation holds for all polynomial orders  $p$ , there are exceptions from this observation (cf.  $\Delta\ell = 1$  and 24 cores) if dynamic adaptivity kicks in. The transferred data starts even to decrease for enclave tasking, while the used bandwidth continues to increase. We assume that this stems from the fact that multilevel transfer operators which combine data from multiple resolutions are part of the skeleton and thus triggered right after another. Some grid data remains in the cache. At the same time, the relative number of enclave cells with their “non-deterministic” memory access reduces.

Our code evaluates  $R$  tasks immediately and makes the solution  $u$  guide the dynamic adaptivity before it spawns background tasks. Consequently, enclave tasking might remove data from the cache due to capacity constraints which is later re-accessed by the  $C$  tasks. The memory access needs however are homogenised as memory access bursts are avoided, and there is no computationally intense phase of  $C$  computations followed by lots of  $R$  tasks.

### 6.3 Manycore shared memory scalability

We rerun the shared memory Broadwell tests on a manycore architecture and observe a smooth runtime behaviour for all setups. Enclave tasking remains superior to a naïve approach

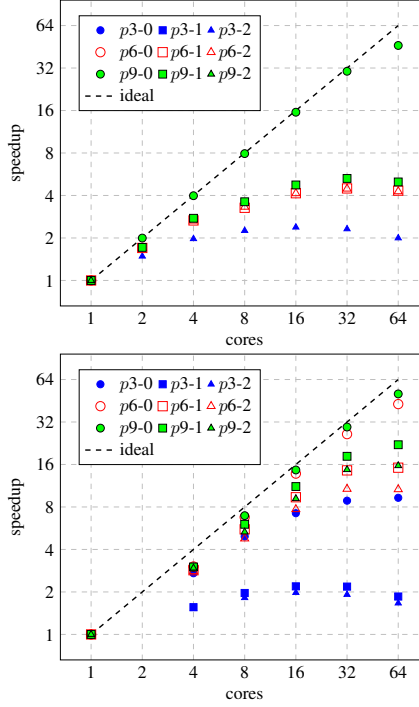


Figure 6: Shared memory speedup on the KNL without enclave tasking (top) and with enclave tasking (bottom).

once dynamic adaptivity is introduced (Figure 6).

A strong scaling saturation is observable unless the order is very high ( $p = 9$  here). Our realisation does profit from deploying two threads to each tile hosting two cores. Using four threads per core in turn is counterproductive for low order discretisations as soon as some dynamic adaptivity is used. It pays off otherwise.

Intel’s manycore architecture is known to benefit from high intensity workloads with very regular data access. For regular grids, it is thus clear that enclave tasking continues to be inefficient in comparison to a plain parallel for. For any setup with dynamic adaptivity and, thus, non-trivial data flow, our results suggest that enclave tasking is a powerful tool. Hereby, the MCDRAM of the KNL which we use in cache mode plus the low baseline frequency make enclave tasking scale smoother than on the Broadwell.

## 6.4 MPI boundary data exchange configuration

Our DG testbed is conceptually well-suited for MPI data transfer as solely cells along the subdomain boundaries exchange face data with their neighbours. Further global communication (time step size exchange, e.g.) is negligible in terms of message footprint. We start with a  $p = 6$  setup where we use 30 ranks which we deploy over 15 nodes, and we distinguish the two different implementations of the boundary exchange: The label SYM exploits that data exchange here is symmetric and issues one `Irecv` per `Isend`. The label IMM identifies a realisation where each outgoing face datum is send away through `Isend` immediately, while `Iprobes` poll the queues whenever a thread is idling. The label AGG finally identifies a third realisation where we aggregate all messages in one buffer and send this buffer away en block at the end of the grid sweep and issues a corresponding receive for its counterpart. This is a popular pattern in HPC and acts as our baseline [8].

Timings first of all clarify that enclave tasking is advantageous for MPI runs (Fig. 7). It increases the opportunity for MPI to transfer data behind the computations. An aggregation of all outgoing messages into one big message pays off for the baseline code without enclaves.

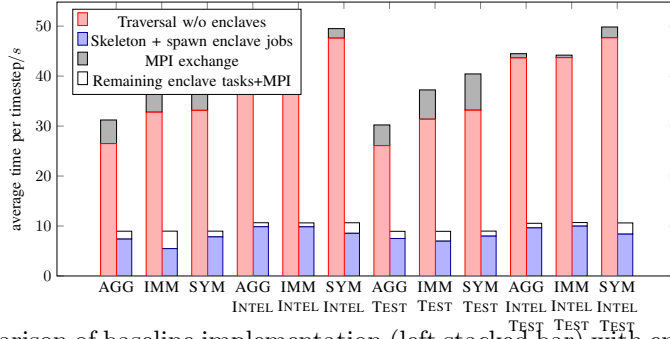


Figure 7: Comparison of baseline implementation (left stacked bar) with enclave partitioning (right stacked bar). Runtimes for (4) with  $p = 6$  on regular grid hosting 182,284,263 dofs on 30 ranks. AGG, IMM, SYM are three different send/receive strategies. INTEL denotes the usage of Intel’s MPI progression thread. TEST denotes manual MPI progression through `Test` calls.

Here, manual MPI progression also is advantageous. Using a dedicated MPI thread is problematic, as it effectively reduces the number of available cores for the computation. Our two proposed MPI data exchange strategies are of no value for aggregated data exchange, which transfers only one big message per grid sweep and thus has minimal MPI message overhead.

Enclave tasking allows the runtime to slot in enclave jobs into phases of the skeleton traversal which exhibit low concurrency. The time spent on the processing of the remaining enclave tasks thus is very short. This time is also used by threads running idle to poll the MPI subsystem. Neither a manual testing of message transfer nor sacrificing a thread to MPI progression is necessary anymore. Both solely induce overhead.

All three exchange patterns perform comparable with enclaves. This does not hold for the Infiniband systems, where we observed a performance break-down for the symmetric data exchange (not shown). The present Omnipath systems are superior in handling large numbers of small incoming messages. Both aggregation and immediate sends with `Iprobe` polling are performant, while the aggregation requires some additional memory buffers as well as manual data movements.

Yet, we emphasise that our late receives are a double-edged sword even if they pay off in terms of runtime: For bigger rank counts and setups, we also observe a significant increase of required memory, as incoming messages might be buffered in the unexpected message queue prior to their `Iprobe` call. Such an effect might be negligible for the Euler equations with only five unknowns. Users of our code base with more complex PDEs however have reported to suffer from these MPI memory footprint increases.

## 6.5 MPI+X upscaling

We wrap up our experiments with some upscaling studies for MPI+TBB on the Ivy Bridge cluster. Besides the  $27 \times 27 \times 27$  grid, we also conducted experiments with a  $81 \times 81 \times 81$  grid to which we added additional AMR levels. They start from  $3.40 \cdot 10^7$  ( $p = 3$ ),  $1.82 \cdot 10^8$  ( $p = 6$ ) or  $5.31 \cdot 10^8$  ( $p = 9$ ) and increase this dof count by more than a factor of seven through additional AMR levels. The best-performing MPI data exchangers have been used.

Our measurements confirm that enclave tasking not only is superior to a naïve approach for a fixed core count, but also preserves good scaling behaviour (cf. Fig. 8 for  $p = 6$  as an example). All measurements group around a linear trend. This trend deviates from a real serial speedup, i.e. a code compiled without any TBB or MPI routines, by a factor of two to three; which is the price we pay for the additional TBB and MPI instrumentation.

Most scaling codes hide communication behind computations and, thus, also avoid bursts of bandwidth demands. Enclave tasking realises this inherently. This is an advantage compared to other codes which manually run through the MPI domain boundary first, then send out all data, and eventually continue with the internal work. These alternative, manual ap-

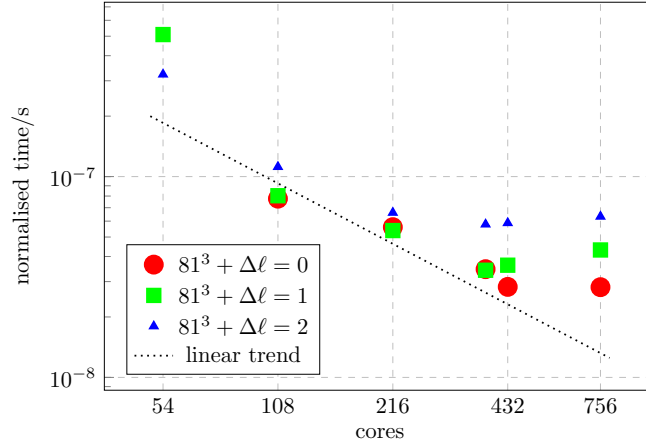


Figure 8: Normalised time (time per dof per grid sweep) for  $p = 6$  on the Ivy Bridge cluster. The trend line denotes a linear speedup.  $\Delta\ell$  denotes the number of added adaptivity levels relative to a base grid of  $81 \times 81 \times 81$ .

proaches naturally suffer if an adaptivity criterion refines around an MPI subdomain boundary. With enclave tasking, the background jobs squeeze into the schedule whenever cores become available. They do not suffer that significantly from delayed or elongated skeleton processing or MPI exchange.

Besides the fact that enclave tasking allows us to merge the MPI data exchange and progression into the tasking, we observe that AMR does not harm the scalability of enclave tasking significantly. Where AMR performs worse, it is due to the absence of proper dynamic load balancing. However, AMR grids even yield lower cost per dof for some smaller core choices. Here, refined grid regions are “more” localised in one subdomain, i.e. the ratio of local skeleton cells to enclave cells reduces. With enclave tasking, the background jobs squeeze into the schedule whenever cores become available. They never delay the actual skeleton processing or MPI exchange, but in turn profit from a reduced skeleton traversal time.

## 7 Conclusion

Enclave tasking is a powerful technique to tune discontinuous Galerkin-type codes relying either on matrix-free evaluations or realising explicit time stepping. It removes multicore synchronisation points and allows the scheduling to overlap computation and communication. The enclave pattern certainly translates into other application areas. It is a powerful method to increase the asynchronism in dynamic AMR.

Our experiences propose some improvements of existing task systems: On the one hand, the results suggest that future task systems would benefit from MPI triggers (guards): tasks become active (ready) once the MPI subsystem flags that there are messages ready to arrive. In theory, such a feature should be supported through hardware. On the other hand, our data suggest that HPC task systems should give the user codes the opportunity to create batches of tasks which are then processed en block even though the task creation is (close to) serial. Finally, we summarise that our implementation could benefit from an MPI implementation where the unexpected message queue is—without manual buffering—automatically handed over to the system upon a receive command, and no memory is “wasted” on this particular queue therefore. Our late receiver-**Iprobe** pattern can be read as a single-sided communication pattern where the receive window is opened upon demand. Future studies will have to uncover whether a straightforward get/put realisation renders our pattern unnecessary, i.e. allows MPI implementations really to transfer data in the background without user interference.

There are natural follow-up steps worth further investigations: First, enclave tasking can-

didates to be used in connection with accelerators. Our terminology is inspired by the work of Sundar and Ghattas [20] who use enclaves to ensure that accelerators processing an enclave do not have to communicate with other accelerators directly. The enclaves are separated by skeleton cells. Our background tasks are perfect candidates to be deployed to accelerators, too. Their data transfers can be hidden behind computation, and the construction of the skeleton mesh ensures that no accelerator has to exchange DG jumps between node boundaries. Second, enclave tasking is tied to the spatial and temporal smoothness of the compute grid. Indeed, many applications will be able to make tasks along resolution boundaries part of the enclaves rather than the skeleton if they know a priori the not dynamic mesh refinement will happen. Follow-up application studies exploiting the technique thus will have to deliver appropriate smoothness predictors that allow the tasking to work as aggressively as possible, i.e. to identify as many background tasks as possible. This notably is important for non-linear problems where refined regions may arise “suddenly” through wave stiffening, e.g. It is an open question how we can even turn around the argument and make grids excessively smooth such that they allow for more aggressive tasking. We exchange increased cell counts with higher scalability and throughput. Finally, our enclave tasking realisation lacks the integration with load balancing metrics.

## Acknowledgements

The authors appreciate support received from the European Unions Horizon 2020 research and innovation programme under grant agreement No 671698 (ExaHyPE). This work made use of the facilities of the Hamilton HPC Service of Durham University. Particular thanks are due to Henk Slim for supporting us with Hamilton. The authors furthermore gratefully acknowledge the Gauss Centre for Supercomputing e.V. ([www.gauss-centre.eu](http://www.gauss-centre.eu)) for funding this project by providing computing time on the GCS Supercomputer SuperMUC at Leibniz Supercomputing Centre ([www.lrz.de](http://www.lrz.de)). Thanks are due to all members of the ExaHyPE consortium who made this research possible. All underlying software is open source [1].

## References

- [1] M. Bader, M. Dumbser, A.A. Gabriel, H. Igel, L. Rezzolla, and T. Weinzierl. ExaHyPE—an Exascale Hyperbolic PDE solver Engine, 2017.
- [2] A. Baggag, H. Atkins, C. Özturan, and D. Keyes. Parallelization of an object-oriented unstructured aeroacoustics solver. 1999.
- [3] M. Berger and P. Colella. Local adaptive mesh refinement for shock hydrodynamics. *Journal of Computational Physics*, 82:64–84, 1989.
- [4] D. Charrier and T. Weinzierl. Stop talking to me—a communication-avoiding ader-dg realisation. 2018. arXiv:1801.08682 (submitted).
- [5] J. Dongarra, J. Hittinger, et al. Applied Mathematics Research for Exascale Computing, 2014. DOE ASCR Exascale Mathematics Working Group: <http://www.netlib.org/utk/people/JackDongarra/PAPERS/doe-exascale-math-report.pdf>.
- [6] A. Dubey, A. S. Almgren, J. B. Bell, M. Berzins, S. R. Brandt, G. Bryan, P. Colella, D. T. Graves, M. Lijewski, F. Löffler, B. O’Shea, E. Schnetter, B. van Straalen, and K. Weide. A survey of high level frameworks in block-structured adaptive mesh refinement packages. *CoRR*, 74(12):3217–3227, 2016.
- [7] M. Dumbser and M. Käser. An arbitrary high-order discontinuous Galerkin method for elastic waves on unstructured meshes - II. The three-dimensional isotropic case. *Geophysical Journal International*, 167(1):319–336, 2006.



- [8] G. Hager and G. Wellein. *Introduction to High Performance Computing for Scientists and Engineers*. CRC Press, Inc., Boca Raton, FL, USA, 1st edition, 2010.
- [9] T. Hoefer and A. Lumsdaine. Message progression in parallel computing - to thread or not to thread? In *2008 IEEE International Conference on Cluster Computing*, pages 213–222, Sept 2008.
- [10] M. Hutchinson, A. Heinecke, H. Pabst, G. Henry, M. Parsani, and D. Keyes. Efficiency of high order spectral element methods on petascale architectures. In J. M. Kunkel, P. Balaji, and J. Dongarra, editors, *High Performance Computing*, pages 449–466, Cham, 2016. Springer International Publishing.
- [11] A. Ilic, F. Pratas, and L. Sousa. Cache-aware roofline model: Upgrading the loft. *IEEE Computer Architecture Letters*, 13(1):21–24, Jan.-June 2014.
- [12] D. Komatitsch, G. Erlebacher, D. Göddeke, and D. Michéa. High-order finite-element seismic wave propagation modeling with MPI on a large GPU cluster. *Journal of Computational Physics*, 229(20):7692–7714, October 2010.
- [13] K. Kormann and M. Kronbichler. Parallel Finite Element Operator Application: Graph Partitioning and Coloring. pages 332–339. IEEE, December 2011.
- [14] M. Kronbichler and K. Kormann. Fast matrix-free evaluation of discontinuous Galerkin finite element operators. *arXiv:1711.03590 [cs, math]*, November 2017. arXiv: 1711.03590.
- [15] M. Kronbichler, K. Kormann, I. Pasichnyk, and M. Allalen. Fast Matrix-Free Discontinuous Galerkin Kernels on Modern Computer Architectures. In J. M. Kunkel, R. Yokota, P. Balaji, and D. Keyes, editors, *High Performance Computing*, volume 10266, pages 237–255. Springer International Publishing, Cham, 2017.
- [16] R. J. LeVeque. *Finite-Volume Methods for Hyperbolic Problems*. Cambridge University Press, 2002.
- [17] A. Pegushin. Have we made task\_group a little too easy to use? Intel Developer Zone, 2010. [https://software.intel.com/en-us/blogs/2010/05/07/have-we-made-task\\_group-a-little-too-easy-to-use](https://software.intel.com/en-us/blogs/2010/05/07/have-we-made-task_group-a-little-too-easy-to-use).
- [18] J. Reinders. *Intel Threading Building Blocks*. O’Reilly & Associates, Inc., first edition, 2007.
- [19] M. Schreiber, T. Weinzierl, and H. J. Bungartz. Cluster Optimization and Parallelization of Simulations with Dynamically Adaptive Grids. In F. Wolf, B. Mohr, and D. Mey, editors, *Euro-Par 2013 Parallel Processing*, volume 8097 of *Lecture Notes in Computer Science*, pages 484–496. Springer, 2013.
- [20] H. Sundar and O. Ghattas. A nested partitioning algorithm for adaptive meshes on heterogeneous clusters. In *Proceedings of the 29th ACM on International Conference on Supercomputing*, ICS ’15, pages 319–328, New York, NY, USA, 2015. ACM.
- [21] Clawpack Development Team. Clawpack software, 2018. Version 5.
- [22] J. Treibig, G. Hager, and G. Wellein. LIKWID: A Lightweight Performance-Oriented Tool Suite for x86 Multicore Environments. In *Proceedings of the 2010 39th International Conference on Parallel Processing Workshops*, ICPPW ’10, pages 207–216. IEEE Computer Society, 2010.

- [23] C. Uphoff, S. Rettenberger, M. Bader, E. H. Madden, T. Ulrich, S. Wollherr, and A. A. Gabriel. Extreme scale multi-physics simulations of the tsunamigenic 2004 sumatra megathrust earthquake. In *Proceedings of the International Conference for High Performance Computing, Networking, Storage and Analysis*, SC '17, pages 21:1–21:16, New York, NY, USA, 2017. ACM.
- [24] S. Williams, A. Waterman, and D. Patterson. Roofline: An insightful visual performance model for multicore architectures. *Commun. ACM*, 52(4):65–76, April 2009.
- [25] M. Wittmann, G. Hager, T. Zeiser, and G. Wellein. Asynchronous MPI for the Masses. *CoRR*, abs/1302.4280, 2013.